Dalton Transactions

Accepted Manuscript

ROYAL SOCIETY OF CHEMISTRY

www.rsc.org/dalton

Journal Name

RSCPublishing

ARTICLE

A Novel Fe/Fe_3O_4/N-carbon composite with hierarchical porous structure and in situ formed N-doped graphene-like layers for high-performance lithium ion batteries†

Cite this: DOI: 10.1039/x0xx00000x

Received 00th January 2012,
Accepted 00th January 2012

DOI: 10.1039/x0xx00000x

www.rsc.org/

Yao Li[a], Qing Meng[b], Shen-min Zhu*[a], Zeng-hui Sun[a], Hao Yang [a], Zhi-xin Chen[b], Cheng-ling Zhu[a], Zai-ping Guo[b] and Di Zhang*[a]

A Fe/Fe_3O_4/N-carbon composite consisting of porous carbon matrix containing a highly conductive N-doped graphene-like network and Fe/Fe_3O_4 nanoparticles was prepared. The porous carbon has hierarchical structure which inherits from rice husk and N-doped graphene-like network formed in situ. When used as an anode material for lithium batteries, the composite delivered a reversible capacity of approximately 610mAh g^{-1} at a current density of 200 mA g^{-1} even after 100 cycles, due to the synergism between the unique hierarchical porous structures, highly electric conductive N-dopped graphene-like networks and nanosized particles of Fe/Fe_3O_4. This work provides a simple approach to prepare N-doped porous carbon activated nanoparticle composite which could be used to improve the electrochemical performance of lithium ion batteries.

1. Introduction

Lithium ion batteries (LIBs) have been extensively used in portable electronic devices as well as electric vehicles, because of their high energy density, long cycle life, low self-discharge and no "memory effect".[1-4] As an essential part of LIBs, anode materials play an important role in the performance of LIBs and thus attract considerable attention. Accordingly, a variety of new anode materials, such as carbon materials, metal alloy, metal oxides, has been developed.[5-7] Among them, iron oxide is considered as an ideal anode material since its adequate theoretical capacity (1004 mA h g^{-1} for α-Fe_2O_3 and 924 mA h g^{-1} for Fe_3O_4), low toxicity, moderate volume change during lithium extraction and insertion processes. However, iron oxide will break into small metal clusters since they can react with Li to form Li_2O, which along with a great volume expansion and a destruction of the structure upon electrochemical cycling, especially at high rates, thus resulting in severe loss of capacity with cycling and a poor electronic conductivity.

Both nanostructure design and composite with porous carbon are useful strategies to improve the reversible capacity and rate capacity. Nanostructure can shorten Li ion insertion/extraction pathways. Composite with porous carbon may buffer volume expansion upon lithium extraction and insertion. Unfortunately, porous carbons involved in the formation of composite are usually amorphous.[8-10] Their low electronic conductivity has to be considered seriously, especially in LIBs system.[11] In order to improve the electronic conductivity, attempts such as introducing graphene-like structures in porous carbon have been made. A graphitized mesoporous carbon produced by CVD has shown a high capacity of about 340 mAh g^{-1} at a rate of 0.1C.[12] The capacity of ~250 mAh g^{-1} was retained after ten cycles. Similarly, a simple catalyzed method was developed for the synthesis of Fe_2O_3/graphitized mesoporous carbon composites, which showed a decent capacity of approximately 623 mAh g^{-1} as well as cycling stability.[13] In addition, nitrogen-doping is proved to be another effective way to enhance the electrochemical properties of carbon composites.[14-17] Nitrogen-doped

carbonaceous materials may offer more active sites and enhance the interaction between carbon and lithium and thus to improve the kinetics of lithium diffusion and transfer.[17] Nitrogen-doped graphene reported in the literature showed an energy density of approximately 199 mAh g^{-1} even under a high current density of 25 A g^{-1}.[18] The incorporation of a carbon material with a porous structure, graphene-like layers, and nitrogen-doping is proposed as a feasible way to improve the electrochemical performance of iron oxides for high performance LIBs.

In this paper, Fe/Fe_3O_4 nanoparticles were embedded into nitrogen doped porous carbon through a simple impregnation then polymerization and calcinations route, generating a novel Fe/Fe_3O_4/carbon composite (Fe/Fe_3O_4/N-carbon). The composite is composed of Fe/Fe_3O_4 nanoparticles and porous carbon with N-doped graphene-like structure. Owing to the high specific capacity of Fe_3O_4, bufferring effective provided by nanostructure and porous carbon composition and the improved electrical conductivity of the electrode by the incorporation of Fe nanoparticles and N-doped graphene-like structure, this Fe/Fe_3O_4/N-carbon showed an enhanced specific capacity and cycling stability.

2. Experimental

2.1 Preparation

Typically, a rice husk precursor was used to fabricate porous carbon (RHC) via carbonization at 650 ºC, followed by activation at 800 °C by KOH. Then, the calcined RHC was washed with 12% HCl and distilled water. Washed RHC (0.5 g) was mixed with 1mL 0.9 M iron chloride ($FeCl_3$) solution. The mixture was exposed in pyrrole vapor at 50 °C for 3 hours, followed by calcination at 850 °C for 2 hours under nitrogen. The product is denoted as Fe/Fe_3O_4/N-carbon. For comparison, the mixture of RHC and iron chloride was treated by the same procedure but without pyrrole vapor exposure. The product fabricated is denoted as Fe/Fe_3O_4/carbon. the pure iron chloride was treated by the same procedure is denoted as Fe/Fe_3O_4/N.

2.2 Characterization

Fourier transform-infrared measurements (FT-IR) were conducted on KBr pellets with a PE Paragon 1000 spectrophotometer. The synthesized samples were characterized by X-ray diffraction (XRD) on a RigakuD/max 2550VL/PC system operated at 35 kV and 200 mA with Cu Kα radiation (λ=1.5406 Å), at a scan rate of 5° min^{-1} and step size of 0.02°. Raman spectroscopy was measured on a Renishawin Via Raman Microscope. X-ray photoelectron spectra (XPS) were collected on a physical electronics PHI5400 using Mg K radiation as X-ray source. All the spectra were corrected with C1s (285.0 eV) band. Elemental analysis was processed using a Vario ELIII/I soprime isotope ratio mass spectrometer. Nitrogen adsorption measurements at 77 K were performed using an ASAP2020 volumetric adsorption analyzer, after the samples had been out gassed for 8 h in the degas port of the adsorption apparatus. Scanning electron microscopy (SEM) was performed on a JEOL JSM-6360LV field emission microscope at 15 kV. Transmission electron microscopy (TEM) was carried out on a JEOL 2010 microscope at 200 kV. Thermal gravimetric analysis (TGA) was conducted on a PE TGA-7 instrument with 20 °C min^{-1}.

2.3. Electrochemical measurements

Electrochemical experiments were carried out in two-electrode Swagelok cells. The working electrodes were made by mixing the Fe/Fe_3O_4/N-carbon composite with carbon black and binder (polyvinylidene fluoride, PVDF) at a mass ratio of 80:10:10. The mixture was then spread uniformly onto a copper foil cylinder with a diameter of 12 mm and dried in vacuum at 80 °C. The net mass loading of activated material for each tested electrode was between 1.0-1.5 mg. The cells were assembled in an argon filled glove box (Mikrouna 1220/750). Metallic lithium foil was used as the counter electrode. The electrolyte was made of 1 M LiPF6 dissolved in the mixture of ethylene carbonate (EC) and diethylene carbonate (DEC) with the volume ratio of 1:1. The charge/discharge profiles of the electrodes were collected at room temperature on a Land CT2001A battery test system. The cyclic voltammetry (CV) curves were obtained on a Chenhua CHI 660D electrochemical workstation in the potential range of 0.05-3.0 V at a scan rate of 0.5 mV s^{-1}. Electrochemical impedance spectra were measured by using a Chenhua CHI 660D electrochemical workstation with an AC voltage signal of 5 mV, in the frequency range between 100 kHz and 5 mHz. For comparison, the electrochemical performances of Fe/Fe_3O_4/carbon were evaluated under the same conditions. The cells were disassembled in the glovebox after 100 cycles, and the working electrode was taken out and washed three times using dimethyl carbonate (DMC) solution. It was then prepared for TEM observation.

3. Results and Discussion

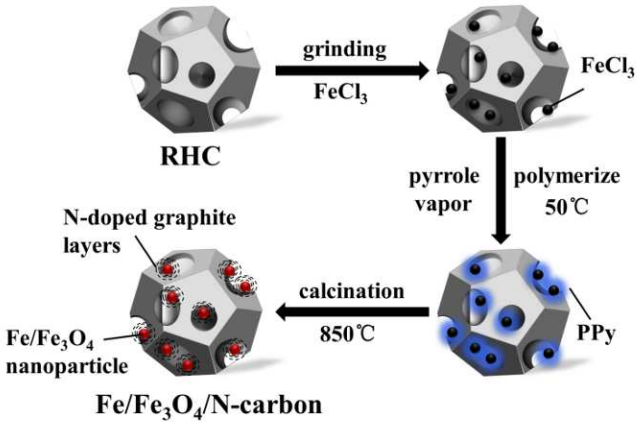

Scheme 1 Schematic illustration of the formation of the Fe/Fe_3O_4/N-carbon composite.

In this work, a Fe/Fe_3O_4/N-carbon composite was synthesized by a three-step method as described in Fig. 1. Firstly, porous carbon fabricated from rice husk (RHC) was pretreated by nitric acid and carboxyl RHC was obtained. Then, the carboxyl RHC was impregnated in a $FeCl_3$ solution, and set in a pyrrole

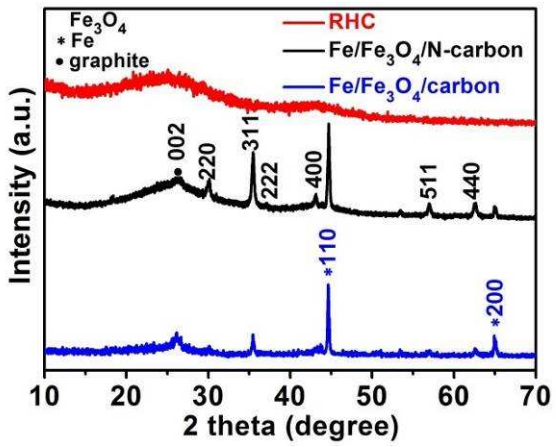

Fig. 1 XRD patterns of RHC, Fe/Fe_3O_4/N-carbon and Fe/Fe_3O_4/carbon.

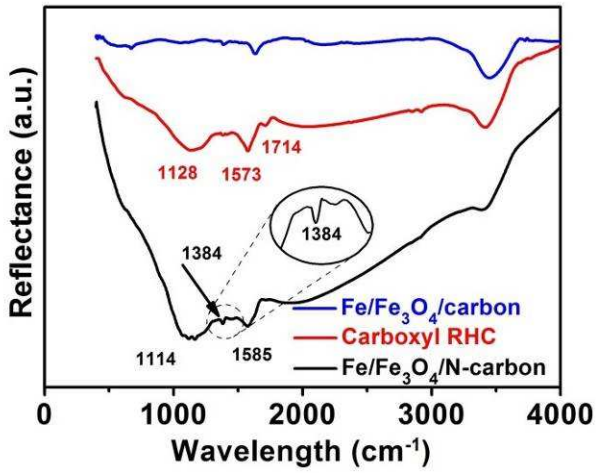

Fig. 2 FTIR spectra of Fe/Fe_3O_4/carbon, Carboxyl RHC and Fe/Fe_3O_4/N-carbon.

vapour environment at 50 °C for 3h, during which pyrrole migrated into the pores of carboxyl RHC and in situ polymerization of pyrrole occurred due to the catalytic effect of the impregnated Fe^{3+}. Finally, calcinations was performed at 850 °C for 2 h, and during this process the polypyrrole may convert into nitrogen doped graphite layers with iron oxide nanoparticles inside.

Fig. 1 shows XRD patterns of RHC, Fe/Fe_3O_4/carbon and Fe/Fe_3O_4/N-carbon. There is a detectable diffraction peak at 26.4° in the XRD pattern of Fe/Fe_3O_4/N-carbon (Fig. 2b, corresponding to an interlayer d spacing of approximately 0.34 nm. It indicates the existence of turbostratic ordering of graphene-like materials, similar to those observed in bulk carbon nitride materials.[16] The diffraction peaks at 30.1°, 35.4°, 43.1°, 56.9° and 62.5°, can be indexed as (220), (311), (400), (511) and (440) of face-centered cubic Fe_3O_4 (JCPDS no. 19-0629), respectively. The diffraction peaks at 44.7° and 65.0° are indexed as (110) and (200) of body-centered cubic Fe, respectively (JCPDS no. 06-0696). The reduction by carbon of

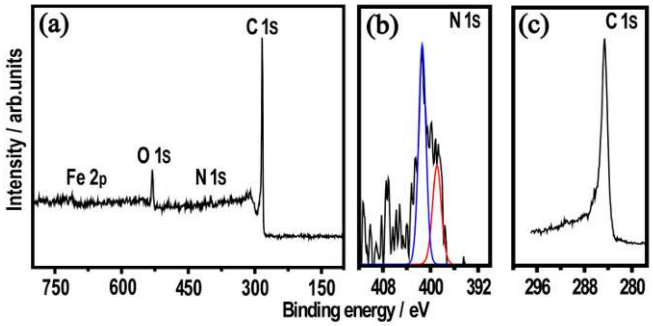

Fig. 3 XPS spectra of Fe/Fe_3O_4/N-carbon.

Fe^{3+} species attached on the surface of RHC at a high temperature of 850 ºC generates the body-centered cubic Fe. Using the Scherrer formula from the width of the diffraction peak at 35.4°, the average size of Fe_3O_4 particles was estimated to be approximately 45 nm. The XRD pattern of Fe/Fe_3O_4/carbon is similar to that of Fe/Fe_3O_4/N-carbon thus Fe and Fe_3O_4 particles are also present in Fe/Fe_3O_4/carbon.

The presence of nitrogen in the Fe/Fe_3O_4/N-carbon composite was investigated by using FT-IR (Fig. 2). The FT-IR spectrum of carboxyl RHC, shows an absorption at 1714 cm^{-1} which is characteristic of C=O stretching vibration, owing to the existence of COOH and an absorption at 1573 cm^{-1} which is attributed to asymmetric -COO- stretching.[20] After calcination, the peak from COOH groups disappeared as evidenced by the spectra of both Fe/Fe_3O_4/N-carbon and Fe/Fe_3O_4/carbon. As compared with Fe/Fe_3O_4/carbon, Fe/Fe_3O_4/N-carbon has two new absorptions: (i) at 1585 cm^{-1}, attributed to N-H in-plane deformation vibrations or C=C stretching vibration, and (ii) at 1384 cm^{-1} which is caused by the presence of C-N stretching vibration in Fe/Fe_3O_4/N-carbon composite.[21] These two extra absorption peaks clearly suggested the presence of nitrogen in Fe/Fe_3O_4/N-carbon.

Raman spectra of RHC, Fe/Fe_3O_4/carbon and Fe/Fe_3O_4/N-carbon were shown in Fig. S1†). Two bands at around 1590 and 1336 cm^{-1} are known as the graphite sp^2 (E_{2g}) carbon band or G band and the defect sp^3 carbon band or D band respectively.[22, 23] For RHC, the D band is significantly higher than the G band: $I_D/I_G>1$, indicating that the high content of the amorphous carbon. The I_D/I_G decreased significantly in Fe/Fe_3O_4/carbon and Fe/Fe_3O_4/N-carbon samples in comparison to that of RHC, indicating the graphitization in both Fe/Fe_3O_4/carbon and Fe/Fe_3O_4/N-carbon samples.[24-27] It should be noted that no band shift was detected for Fe/Fe_3O_4/carbon in comparison with RHC. However, a distinct G band p-shift of 12 cm^{-1} was observed for the sample of Fe/Fe_3O_4/N-carbon, which could be explained by the N-doping of the composite, as reported by others.[27]

The composition of Fe/Fe_3O_4/N-carbon was further investigated by XPS measurement. As expected, all the peaks present in the spectrum (Fig. 3a) can be assigned to carbon (C 1s), nitrogen (N 1s), iron (Fe $2p^3$) and oxygen (O 1s). There are two binding energy peaks in the N 1s pattern (Fig. 3b). The peak at 397.8 eV is assigned to sp^2 hybridized N atoms bonded to carbon atoms, and that at 400.2 eV corresponds to pyrrolic N atoms trigonally bonded with sp^2 or sp^3 hybridized carbon atoms.[28] The XPS analyses confirm the existence of pyrrolic nitrogen in the porous composite and are consistent with the C 1s spectrum (Fig. 3c).

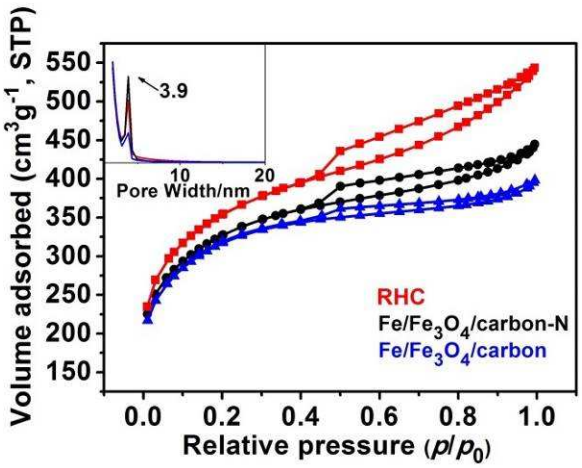

Fig. 4 N_2 adsorption isotherms of RHC, Fe/Fe_3O_4/carbon and Fe/Fe_3O_4/N-carbon.

Nitrogen adsorption/desorption was conducted to characterize the porous structures (Fig. 4). The specific surface area of the RHC matrix and Fe/Fe_3O_4/carbon are approximately 1245 and 1116 m^2 g^{-1}, respectively, suggesting that the impregnation and calcination give little effect on the surface area. More interestingly the resultant Fe/Fe_3O_4/N-carbon still has a surface area of 1151m^2 g^{-1} (Fig. 4), indicating the existence of pyrrole vapor did not influence the porous structures. All the samples show a hysteresis loop in the P/P_0 range of 0.45-1.0, and the pore width was around 3.9 nm. The results clearly suggest that the large specific surface area and hierarchical microstructures of RHC were retained in Fe/Fe_3O_4/N-carbon and Fe/Fe_3O_4/carbon. These hierarchical structures would provide a buffering room for volume change and necessarily accessible channels for charge transfer during charge-discharge cycles.

The microstructures of Fe/Fe_3O_4/N-carbon and RHC were compared in Fig. 5. The porous and hierarchical structure of RHC matrix is clearly revealed in the secondary electron images given in Figs. 5a and b. The hierarchical structure of RHC was retained in the sample of Fe/Fe_3O_4/N-carbon as shown in Figs. 6c and d. Obviously, the iron oxide nanocomposite existed homogeneously on the porous carbon matrix in Fe/Fe_3O_4/N-carbon and Fe/Fe_3O_4/carbon. As determined by thermogravimetric analysis (TGA) (Fig. S2†), the weight of Fe/Fe_3O_4/N was increased during the thermogravimetric analysis since the oxidation process of Fe and Fe_3O_4 to Fe_2O_3. Depend on the mass increased ratio of 8 wt.% , the weight percentages of Fe and Fe_3O_4 are calculated as 88.5 wt.% and 11.5 wt.% in Fe/Fe_3O_4/N, respectively. Thus, the mass residual of Fe/Fe_3O_4/N-carbon and Fe/Fe_3O_4/carbon being 26 wt.% and 30 wt.%, means carbon content in Fe/Fe_3O_4/N-carbon and Fe/Fe_3O_4/carbon is around 76 wt.% and 72 wt.%, respectively.

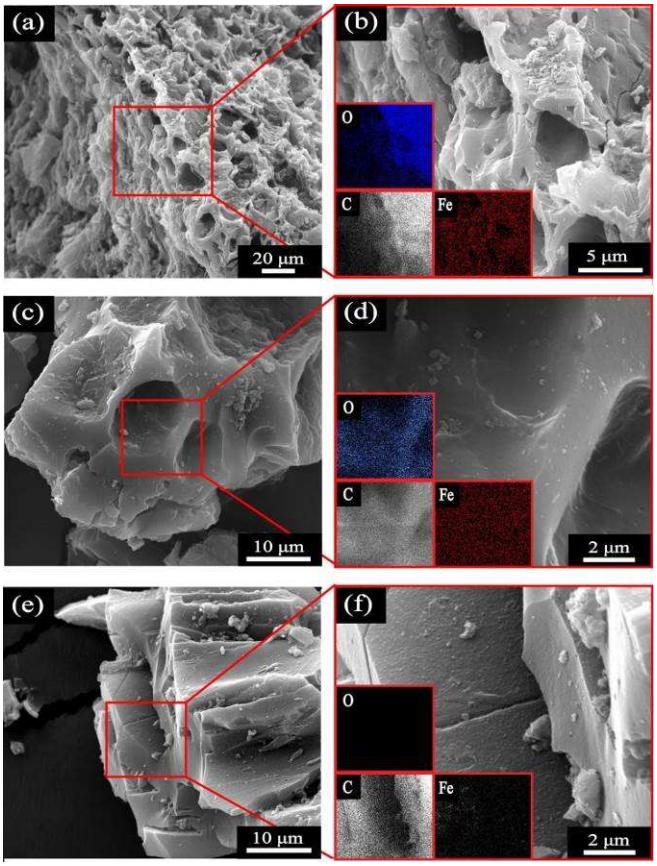

Fig. 5 SEM micrographs and mapping photograph (insert) of (a,b)Fe/Fe_3O_4/N-carbon (c,d)Fe/Fe_3O_4/carbon composite and (e,f)RHC matrix.

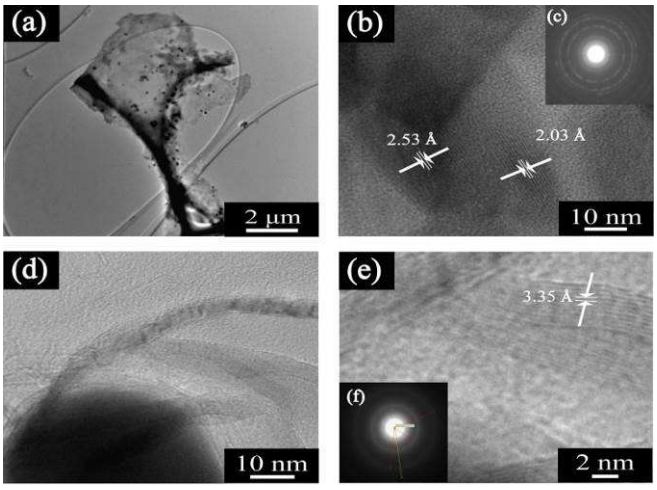

Fig. 6 TEM images and SAED pattern of Fe/Fe_3O_4/N-carbon composite.

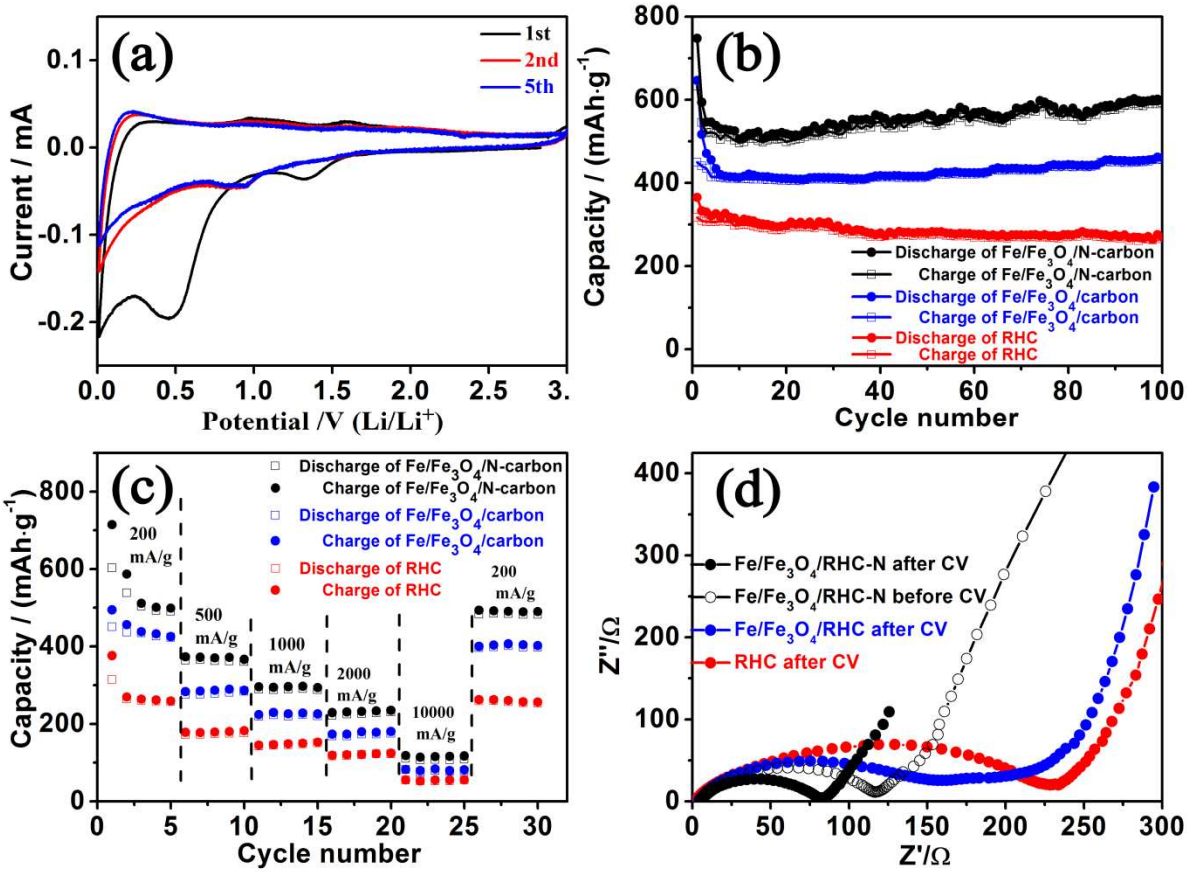

Fig. 7 (a)CV curves of Fe/Fe_3O_4/N-carbon. (b) Capacity versus cycle number plots of Fe/Fe_3O_4/N-carbon, RHC and Fe/Fe_3O_4/carbon in the voltage range of 0.1-3.0 V at a current density of 200 mA g^{-1}. (c)Rate capability of Fe/Fe_3O_4/N-carbon, RHC and Fe/Fe_3O_4/carbon. (d)Nyquist plots of Fe/Fe_3O_4/N-carbon, Fe/Fe_3O_4/carbon and RHC obtained by applying a sine wave with an amplitude of 5.0 mV over the frequency range from 100 kHz to 0.01 Hz.

Transmission electron microscopy (TEM) images of Fe/Fe_3O_4/N-carbon are shown in Fig. 6. Particles less than 100 nm are dispersed on the RHC matrix (Fig. 6a). These nanoparticles may be either Fe_3O_4 or Fe nanoparticles in the frame work formed during calcination process, which have been confirmed by XRD. The average particle size is estimated to be around 47 nm (Fig. 6b), which is consistent with that of the XRD analysis. The crystal structure of Fe/Fe_3O_4 nanoparticles is revealed by the HRTEM images in Fig. 4b. The lattice spacings of 2.53 Å and 2.03 Å are ascribed to the (311) plane of Fe_3O_4 and the (110) plane of Fe, respectively. The presence of weak and large rings in the SAED pattern (Fig. 6c) for Fe/Fe_3O_4/N-carbon is evidence for the loss of sample crystallinity, in agreement with the XRD data. A randomly selected nanoparticle magnified in Fig. 6d indicated that it is wrapped by thin graphene-like layers of 5-10 nm in thickness. Further investigation of this graphene-like layers found that the inter planar distance is about 0.34 nm (Fig. 6e), consisting of 5-20 graphene-like layers. The correspondingly SAED pattern also showed in Fig. 6f. The graphene-like layers were likely formed from the pyrrole vapour or other carbonaceous gasses resulted from the decomposition of rice husks with the aid of catalytic iron oxide or iron during the calcination at 800 °C. These well graphitized interconnect frame networks would provide a good electronic conductivity to the composite.

The cyclic voltammogram(CV) curves of Fe/Fe_3O_4/N-carbon composite for the first two and fifth cycles in the voltage range from 3.0 to 0.01 V at a scan rate of 0.01 mV s^{-1} are shown in Fig. 7a. Two reduction peaks are observed in the first cathodic scan of both Fe/Fe_3O_4/N-carbon. The peak at around 0.44V, which are absent in the second cycle, is ascribed to the possible irreversible formation of solid electrolyte interface (SEI) film.[29, 30] The other at around 1.30 V indicates an irreversible reduction of Fe^{3+} to Fe^{2+}.[24] The anodic curves also have two peaks which are centered at about 1.59V and 0.98V, corresponding to the reversible oxidation of Fe^0 to Fe^{3+}or Fe^{2+}, respectively.[31, 32] The peak intensity and integral areas of the fifth cycle are close to that of the second one. These results indicate that the electrochemical reversibility of Fe/Fe_3O_4/N-carbon are gradually built after the initial cycle.

The discharge/charge profiles for the first, the 2nd and the 30th cycles at 50 mA g^{-1} are given in Fig. S3†. Fe/Fe_3O_4/N-carbon shows a first-cycle insertion capacity of 748 mAh g^{-1} and a de-insertion capacity of 633 mAh g^{-1}, corresponding to a

Columbic efficiency of 85 %. The second discharge and charge capacities are 594 and 545 mAh g^{-1}, respectively, with the Columbic efficiency over 91 %. Fe/Fe_3O_4/carbon shows a first-cycle insertion capacity of 647 mAh g^{-1} and a de-insertion capacity of 450 mAh g^{-1}, corresponding to a Columbic efficiency of 70 %. The second discharge and charge capacities are 517 and 440 mAh g^{-1}, respectively, with the Columbic efficiency over 85%. The incorporation of porous carbon with N-doped graphene-like structure significantly improve the electrochemical performance of iron oxides.

The cycling performance of Fe/Fe_3O_4/N-carbon, Fe/Fe_3O_4/carbon and RHC as anode materials for lithium ion batteries at the current density of 200 mA g^{-1} was evaluated and the results are shown in Fig. 7b. The reversible capacity of Fe/Fe_3O_4/N-carbon is ~703 mAh g^{-1} in the first cycle and then stabilizes at ~510 mAh g^{-1} after 10 cycles. Interestingly, the capacity gradually increased to ~610 mAh g^{-1} after 100 cycles. The reversible capacity of Fe/Fe_3O_4/carbon was ~647 mAh g^{-1} in the first cycle and then stabilized at ~413 mAh g^{-1} after 10 cycles and then gradually increased to ~460 mAh g^{-1}. This special phenomenon, of the increase in capacity with cycling, can be attributed to the activating process of the porous anode as reported in Huang's work.[16] However, the porous RHC matrix did not show similar phenomenon when evaluated in the same condition. Thus the increase of the capacity with cycling must be the consequence of activating process of the N doping and iron oxide nanoparticles. The low reversible capacity (~260 mAh g^{-1}) of RHC matrix under the same condition also confirm the validity of N doping and activated nanoparticle association by facile treatment.[16, 18, 33, 34] Among these two factors, the N-doping is the main because the capacity increase is ~100 mAh g^{-1} for Fe/Fe_3O_4/N-carbon and ~47 mAh g^{-1} for Fe/Fe_3O_4/carbon respectively.

Fig. 7c presents the rate performance of Fe/Fe_3O_4/N-carbon at current densities of 200, 500, 1000, 2000 and 10000 mA g^{-1}, and the reversible specific capacity of 507, 301, 293, 233 and 116 mAh g^{-1} are obtained respectively. Even at a higher current density of 10000 mA g^{-1}, the reversible specific capacity is still above 116 mAh g^{-1}. The reversibility is demonstrated by the fact that a high capacity 491 mAh g^{-1} is reached again once the rate is lowered back to 200 mA g^{-1}. However Fe/Fe_3O_4/carbon has the reversible capacity of 405 mAh g^{-1} at the current density of 200 mA g^{-1}, which is about 20% lower than that of the N-doped counterpart. A reversible capacity of 264mAh g^{-1} for RHC has been obtained upon varying the discharge rate from 200 to 10000 and then back to 200 mA g^{-1}. Therefore, not only the rate performance of Fe/Fe_3O_4/N-carbon is much better than that of either Fe/Fe_3O_4/carbon or RHC, but a higher capacity can be reached at a much higher rate.

The electrochemical impedance spectra (EIS) studies of Fe/Fe_3O_4/N-carbon, Fe/Fe_3O_4/carbon and RHC after 5 cycles and Fe/Fe_3O_4/N-carbon before cycles (Fig. 7d) were performed on a Chenhua CHI 660D electrochemical workstation. The Nyquist plots of Fe/Fe_3O_4/N-carbon, Fe/Fe_3O_4/carbon and RHC after 5 cycles and Fe/Fe_3O_4/N-carbon before cycles show a semicircle in the high frequency range and a sloping straight line in the low frequency range. The equivalent circuit of the electrodes is shown in Fig. S4† where Rel, CPE, Rct, W are denoted as solution resistance, double layer capacitance, charge-transfer resistance and Warburg impedance, respectively. The charge-transfer resistance (R_{ct}) of the Fe/Fe_3O_4/N-carbon is calculated to be approximately 81.1 Ω after 5 cycles from 117.8 Ω, much lower than that of the Fe/Fe_3O_4/carbon and RHC electrode electrode (approximately 162.3 and 228.6Ω). The decreased resistance of the Fe/Fe_3O_4/N-carbon electrode is attributed to in situ graphene-like layers and Fe nanoparticles with excellent electrical conductivity.

The microstructure variation of Fe/Fe_3O_4/N-carbon after 100 discharge-charge cycles were examined using TEM (Fig. S5†). Obviously, no aggregation occurred and the nanoparticles are observed dispersing well after cycling. This structure observation of Fe/Fe_3O_4/N-carbon is well consistent with its cycling performance.

Consequently, the low resistance leads to the significantly enhanced rate capability of the Fe/Fe_3O_4/N-carbon composite.
It is known that the depth of lithium ion intercalation and de-intercalation in the non-graphitic carbonaceous materials strongly depends on the anode composition and structure such as crystalline phase, hydrogen content, microstructure and micromorphology.[5, 35-38] As demonstrated by Zhou et al.[39] that large and ordered pore arrays are very beneficial to the intercalation of lithium, which is known as a slow bulk-phase reaction. The hierarchical structure of our Fe/Fe_3O_4/N-carbon composite are readily accessed by the electrolyte solution; that is, Li^+ ions can freely move into large pores and intercalate into the thin pore walls and the N-loading location. Therefore, the high reversibility of Li storage is probably due to the following reasons. (i) The grain size of the activated nanoparticles is less than 50 nm, which limits the anode volume change and reduces the path for Li^+ transportation. (ii) Porous carbon prevents the aggregation of activated nanoparticles. (iii) Graphene-like networks, N-doping and the generation of Fe nanoparticles increase electronic conductivity. (iv) N-doping increases the potential Li^+ insertion locations during discharge and charge. (v) The hierarchical structure with a high surface area provides a large electrode/electrolyte contact area and a favorable pore texture for electrolyte impregnation, thus improving the anode performance. Our results clearly demonstrate that Fe/Fe_3O_4/N-carbon prepared by divertive fabrication is a promising candidate for anode materials of high reversible capacity, good cycle performance and high rate discharge/charge capability in used LIBs.

4. Conclusions

Nitrogen-doped porous carbon containing activated nanoparticles and graphene-like layers was synthesized by a simple impregnation then polymerization and calcination method. The resultant composite Fe/Fe_3O_4/N-carbon has a hierarchical porous structure of rice husk and contains N-doped graphene-like networks and Fe&Fe_3O_4 nanoparticles and has a

high specific surface area of 1151 m^2 g^{-1}. When used as anode in LIB, it showed a high discharge capacity of 610 mAh g^{-1} at 200 mA g^{-1} after 100 cycles and a high rate performance. Considering the abundant hierarchical structures in nature, the strategy here reported is expected to be extended for design and fabrication of other anode materials with unique structures and composition.

Acknowledgements

The authors gratefully acknowledge financial support for this research from the Morgan Crucible Company, the National Science Foundation of China (Nos. 51072117, 51171110), National Basic Research Program of China (973 Program) (No. 2012CB619600), Shanghai Science and Technology Committee (No. 0JC1407600). We also thank Shanghai Jiao Tong University (SJTU) Instrument Analysis Center for material analyses.

Notes and references

[a] State Key Laboratory of Metal Matrix Composites, Shanghai Jiao Tong University, Shanghai 200240, China. E-mail: smzhu@sjtu.edu.cn (S.M. Zhu); Tel: +86 21 3420 2584; Fax: +86 21 3420 2749.

[b] The Faculty of Engineering and Information Science, University of Wollongong, NSW 2522, Australia

† Electronic Supplementary Information (ESI) available: Raman spectra, TGA and Galvanostatic charge–discharge curves curves of RHC, Fe/Fe_3O_4/ carbon and Fe/Fe_3O_4/N-carbon and TEM images of Fe/Fe_3O_4/N-carbon composite after 100 discharge/charge cycles. See DOI: 10.1039/b000000x/

1 J. B. Goodenough and Y. Kim, *Chem. Mater.*, 2009, **22**, 587-603.
2 V. Etacheri, R. Marom, R. Elazari, G. Salitra and D. Aurbach, *Energy Environ. Sci.*, 2011, **4**, 3243-3262.
3 S. S. Zhang, *J. Power Sources*, 2006, **162**, 1379-1394.
4 J. W. Fergus, *J. Power Sources*, 2010, **195**, 939-954.
5 Y. P. Wu, E. Rahm and R. Holze, *J. Power Sources*, 2003, **114**, 228-236.
6 L. Ji, Z. Lin, M. Alcoutlabi and X. Zhang, *Energy Environ. Sci.*, 2011, **4**, 2682-2699.
7 X. T. Chen, K. X. Wang, Y. B. Zhai, H. J. Zhang, X. Y. Wu, X. Wei and J.-S. Chen, *Dalton T.*, 2014, **43**, 3137-3143.
8 Y. Guo, S. Yang, K. Yu, J. Zhao, Z. Wang and H. Xu, Mater. Chem. Phys., 2002, 74, 320-323.
9 D. Kalderis, S. Bethanis, P. Paraskeva and E. Diamadopoulos, Bioresource Technol., 2008, 99, 6809-6816.
10 T. H. Liou, Carbon, 2004, 42, 785-794.
11 M. Endo, C. Kim, K. Nishimura, T. Fujino and K. Miyashita, *Carbon*, 2000, **38**, 183-197.
12 Z. Wu, W. Li, Y. Xia, P. Webley and D. Zhao, *J. Mater. Chem.*, 2012, **22**, 8835-8845.
13 Y. Li, C. Zhu, T. Lu, Z. Guo, D. Zhang, J. Ma and S. Zhu, *Carbon*, 2013, **52**, 565-573.
14 K. Xiao, Y. Liu, P. a. Hu, G. Yu, Y. Sun and D. Zhu, *J. Am. Chem. Soc.*, 2005, **127**, 8614-8617.
15 R. Czerw, M. Terrones, J. C. Charlier, X. Blase, B. Foley, R. Kamalakaran, N. Grobert, H. Terrones, D. Tekleab, P. M. Ajayan, W. Blau, M. Rühle and D. L. Carroll, *Nano Lett.*, 2001, **1**, 457-460.
16 L. Qie, W. Chen, Z. Wang, Q. Shao, X. Li, L. Yuan, X. Hu, W. Zhang and Y. Huang, *Adv. Mater.*, 2012, **24**, 2047-2050.
17 H. Wang, C. Zhang, Z. Liu, L. Wang, P. Han, H. Xu, K. Zhang, S. Dong, J. Yao and G. Cui, *J. Mater. Chem.*, 2011, **21**, 5430-5434.
18 Z. Wu, W. Ren, L. Xu, F. Li and H. Cheng, *Acs Nano*, 2011, **5**, 5463-5471.
19 X. Jin, V. V. Balasubramanian, S. T. Selvan, D. P. Sawant, M. A. Chari, G. Q. Lu and A. Vinu, *Angew. Chem. Int. Ed.*, 2009, **48**, 7884-7887.
20 M. M. Joshi, N. K. Labhsetwar, P. A. Mangrulkar, S. N. Tijare, S. P. Kamble and S. S. Rayalu, *Appl. Catala. A-Gen.*, 2009, **357**, 26-33.
21 M. Lasperas, T. Llorett, L. Chaves, I. Rodriguez, A. Cauvel and D. Brunel, *Stud. Surf. Sci. Catal.*, 1997, **108**, 75-82.
22 M. A. Pimenta, G. Dresselhaus, M. S. Dresselhaus, L. G. Cancado, A. Jorio and R. Saito, *Phys. Chem. Chem. Phys.*, 2007, **9**, 1276-1290.
23 C. Thomsen and S. Reich, *Phys. Rev. Lett.*, 2000, **85**, 5214-5217.
24 L. M. Malard, M. A. Pimenta, G. Dresselhaus and M. S. Dresselhaus, *Physics Reports*, 2009, **473**, 51-87.
25 Y. Lin, C. Lin and P. Chiu, *Appl. Phys. Lett.*, 2010, **96**, 133110-133113.
26 DasA, PisanaS, ChakrabortyB, PiscanecS, S. K. Saha, U. V. Waghmare, K. S. Novoselov, H. R. Krishnamurthy, A. K. Geim, A. C. Ferrari and A. K. Sood, *Nat. Nano*, 2008, **3**, 210-215.
27 X. Wang, X. Li, L. Zhang, Y. Yoon, P. K. Weber, H. Wang, J. Guo and H. Dai, *Science*, 2009, **324**, 768-771.
28 J. Wang, D. N. Tafen, J. P. Lewis, Z. Hong, A. Manivannan, M. Zhi, M. Li and N. Wu, *J. Am. Chem. Soc.*, 2009, **131**, 12290-12297.
29 L. Su, Y. Zhong and Z. Zhou, *J. Mater. Chem.*A, 2013, **1**, 15158-15166.
30 C. Lei, F. Han, D. Li, W.C. Li, Q. Sun, X. Q. Zhang and A.H. Lu, *Nanoscale*, 2013, **5**, 1168-1175.
31 P. Lian, X. Zhu, H. Xiang, Z. Li, W. Yang and H. Wang, *Electrochim. Acta*, 2010, **56**, 834-840.
32 M. Ren, Z. Zhou, Y. Li, X. P. Gao and J. Yan, *J. Power Sources*, 2006, **162**, 1357-1362.
33 L. G. Bulusheva, A. V. Okotrub, A. G. Kurenya, H. Zhang, H. Zhang, X. Chen and H. Song, *Carbon*, 2011, **49**, 4013-4023.
34 F. Su, C. K. Poh, J. S. Chen, G. Xu, D. Wang, Q. Li, J. Lin and X. W. Lou, *Energy Environ. Sci.*, 2011, **4**, 717-724.
35 F. Bonino, S. Brutti, P. Reale, B. Scrosati, L. Gherghel, J. Wu and K. Müllen, *Adv. Mater.*, 2005, **17**, 743-746.
36 J. Liwen and Z. Xiangwu, *Nanotechnology*, 2009, **20**, 155705.
37 T. Zheng, Q. Zhong and J. R. Dahn, *J. Electrochem. Soc.*, 1995, **142**, L211-L214.
38 G. Zhou, D.-W. Wang, X. Shan, N. Li, F. Li and H.-M. Cheng, *J. Mater. Chem.*, 2012, **22**, 11252-11256.
39 H. Zhou, S. Zhu, M. Hibino, I. Honma and M. Ichihara, *Adv. Mater.*, 2003, **15**, 2107-2111.

A Novel Fe/Fe_3O_4/N-carbon composite with hierarchical porous structure and in situ formed N-doped graphene-like layers for high-performance lithium ion batteries

Yao Li[a], Qing Meng[b], Shen-min Zhu*[a], Zeng-hui Sun[a], Hao Yang[a], Zhi-xin Chen[b], Cheng-ling Zhu[a], Zai-ping Guo[b] and Di Zhang*[a]

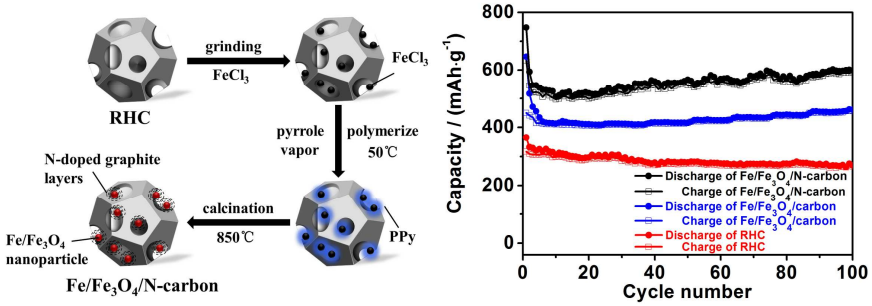

A Fe/Fe_3O_4/N-carbon composite consisting of porous carbon matrix containing a highly conductive N-doped graphene-like network and Fe/Fe_3O_4 nanoparticles was prepared. The porous carbon has hierarchical structure which inherits from rice husk and N-doped graphene-like network formed in situ. When used as an anode material for lithium batteries, the composite delivered a reversible capacity of approximately 610mAh g^{-1} at a current density of 200 mA g^{-1} even after 100 cycles, due to the synergism between the unique hierarchical porous structures, highly electric conductive N-dopped graphene-like networks and nanosized particles of Fe/Fe_3O_4. This work provides a simple approach to prepare N-doped porous carbon activated nanoparticle composite which could be used to improve the electrochemical performance of lithium ion batteries.